http://dx.doi.org/10.5935/0103-5053.20160201

J. Braz. Chem. Soc., Vol. 28, No. 4, 582-588, 2017.
Printed in Brazil - ©2017 Sociedade Brasileira de Química
0103 - 5053 $6.00+0.00

Article

Non-Synergistic UV-A Photocatalytic Degradation of Estrogens by Nano-TiO_2 Supported on Activated Carbon

*Suzamar M. C. Rosa, Arlene B. S. Nossol, Edson Nossol, Aldo J. G. Zarbin and Patricio G. Peralta-Zamora**

Departamento de Química, Universidade Federal do Paraná, CP 19032, 81531-980 Curitiba-PR, Brazil

Many studies have reported significant improvements in the photocatalytic degradation capacity of TiO_2 immobilized in carbonaceous materials, mainly due to a well-characterized synergistic effect. The photocatalytic degradation of the estrogens 17β-estradiol and 17α-ethynylestradiol was evaluated using 1 mg L^{-1} aqueous solutions, employing a nanocomposite containing TiO_2 and activated carbon (TiO_2-AC) prepared by sol-gel technique. The synthesized materials were characterized by thermogravimetric analysis (TGA), X-ray diffraction (XRD), Raman spectroscopy and scanning electron microscopy (SEM). These techniques allowed to estimate the carbon proportion (11.4 wt.%), the phase composition (anatase: 80.2%, brookite: 14.0%, and rutile: 5.8%) and the superficial morphology. Using UV-A radiation provided by a high pressure mercury vapor lamp (125 W) and the synthesized photocatalysts, it was observed the almost complete removal of both estrogens in times shorter than 10 minutes. Considering the similarity between the degradation percentage of nanocomposites (TiO_2 and TiO_2-AC), no synergistic effects between AC and TiO_2 could be assumed.

Keywords: titanium dioxide/activated carbon, nanocomposite, photocatalysis, estrogens

Introduction

Over the last two decades, many studies have demonstrated the high degradation capacity of advanced oxidation processes (AOPs). In general, homogeneous[1] and heterogeneous systems[2] promote fast degradation of resistant substrates, mainly due to the high oxidizing capacity of the *in situ* generated hydroxyl radical.[3]

In the context of the AOPs, heterogeneous photocatalysis occupies a prominent place, particularly when assisted by titanium dioxide.[4] Many recalcitrant organic pollutants have been efficiently degraded by TiO_2-photocatalysis, including azo dyes,[5] pharmaceuticals[6] and estrogens.[7] Typically, the process is applied as slurry systems, consisting in a suspension of fine powdered TiO_2. Because of these characteristics, the separation of the catalyst is expensive and time demanding, which often causes a significant reduction in the benefits of the usual mineralization of the organic substrates.[8]

To overcome this negative aspect, the use of immobilized photocatalysts has been proposed since 1993.[8] Many chemical and physical methods have been employed to prepare TiO_2 coatings on various supports, such as glass,[9] silica,[10] zeolite,[11] among other materials. The sol-gel method and the subsequent thermal treatment usually leads to highly crystalline anatase TiO_2,[12] proving to be a simple and reliable alternative for preparation of mechanically stable TiO_2 films.[13]

Combinations between TiO_2 and carbonaceous materials have been widely explored since the 1990s, with results that demonstrate significant synergistic effects that increase the catalytic activity.[14] In this context, the use of activated carbon (AC) is particularly attractive, because of providing a high surface area for distribution and immobilization of TiO_2.[14] According to the current literature, the synergistically enhanced photocatalytic activity observed with the use of TiO_2-AC composites may be explained by the high adsorption capacity of AC and by the consequent enrichment of target molecules around the catalyst.[14-17] Although the positive effect of AC on the photocatalytic efficiency of TiO_2 is observed with simple mechanical mixtures,[18] it is admitted that the synergetic effect can be maximized by a more intimate contact between the components, which can normally be achieved by the sol-gel technique.[14]

*e-mail: zamora@ufpr.br

In general, it was observed that several studies address on the photocatalytic degradation of emerging contaminants, which represent a wide range of compounds produced naturally or synthetically (i.e., steroid hormones, pesticides, personal care products).[19] Moreover, there are few reports about the degradation of estrogens employing TiO_2-AC. Natural (estrone-E1, 17β-estradiol-E2 and estriol-E3) and synthetic (17α-ethynylestradiol-EE2) hormones are the most commonly steroid hormones found in aquatic ecosystems, mainly because of incomplete removal during wastewater treatment processes.[20] Consequently, the proposal of new treatment technologies appears relevant to remove estrogens from sewage treatment plants effluents and to avoid the potential risks caused by their presence in aquatic environments.

Therefore, the aim of the present work was to investigate the photocatalytic degradation of natural (17β-estradiol-E2) and synthetic (17α-ethynylestradiol-EE2) estrogens in aqueous solution in presence of catalyst Degussa P25 (commercial TiO_2), sol-gel TiO_2 or AC-TiO_2 composite (20% activated carbon).

Experimental

Chemicals

Commercial nanosized titanium dioxide powder, TiO_2-P25 (80 wt.% anatase/20 wt.% rutile by X-ray diffraction, BET surface area of 50 $m^2 g^{-1}$), was purchased from Degussa-Hüls AG. Activated carbon (AC) with 1-2 mm of diameter, large pore size distribution and specific surface area of approximately 800 $m^2 g^{-1}$, was obtained from BRASILAC and previously sieved between 50 and 390 mesh. The organic solvents, methanol (CH_3OH, JT Baker) and acetonitrile (C_2H_3N, Panreac) were of HPLC grade.

Stock solutions (1,000 mg L^{-1}) of the model substrates (17β-estradiol-E2, Sigma-Aldrich, 98%, and 17α-ethynylestradiol-EE2, Sigma-Aldrich, 99%) were prepared in acetonitrile. Working samples (1 mg L^{-1}) were prepared in ultrapure water (Millipore system, resistivity of 18 MΩ cm). The chemical structure of the estrogens is shown in Figure 1.

Sodium hydroxide (0.1 mol L^{-1}, Biotec) and hydrochloric acid (0.1 mol L^{-1}, Qhemis) were used to adjust the pH. Micro glass fiber filters (Macherey-Nagel) of 0.6 μm pore size were used to remove remaining particles from the solutions of estrogens. The other reagents such as titanium isopropoxide, $Ti[OCH(CH_3)_2]_4$, (Acros Organics) and 2-propanol (Panreac) were of analytical grade.

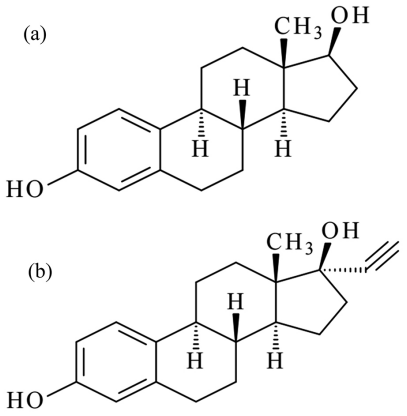

Figure 1. Chemical structure of (a) 17β-estradiol-E2 and (b) 17α-ethynylestradiol-EE2.

Synthesis of nanomaterials

TiO_2 nanoparticles were prepared at ambient temperature by the sol-gel method, according to procedures adapted from Oliveira *et al.*[21] (Figure S1). Step 1: in a glovebox (under argon atmosphere) a mixture containing 20 mL of titanium isopropoxide and 20 mL of 2-propanol was added dropwise to a solution containing HCl (120 mL, 0.2 mol L^{-1}). Step 2: to obtain the gel, the precipitate of the first step was kept on reflux system at 60 °C during 8 h. To obtain a dry gel, the 2-propanol and water were evaporated at 80 °C. The material obtained was denominated sol-gel TiO_2.

The TiO_2-AC nanocomposite was obtained in a similar way, adding a weighed amount of AC (20% of the expected mass of TiO_2) before the formation of the precipitate (step 1, Figure S1).

Characterization techniques

Powder X-ray diffraction patterns were recorded on a Shimadzu XRD-6000 apparatus, with Cu Kα radiation (λ = 1.5418 Å) at 40 kV and 30 mA. The XRD patterns were collected over the 2θ range 10°-80°, at a scan rate of 2° min^{-1}. The mean crystallite size (d) was estimated based on the Scherrer's equation.[22] The materials phase composition ratio was calculated using the equations proposed by Zhang and Banfield.[23]

Raman spectra were recorded on a Renishaw Raman-Image spectrophotometer. A He-Ne laser (λ = 514.5 nm) was used with 2 mW incidence potency over the 200-3000 cm^{-1} region. The relative intensities of bands D and G (I_D/I_G) were calculated according to Wang *et al.*[24]

The morphology and structure of the samples were verified by scanning electron microscopy using a Mira FEG-SEM (TESCAN) equipped with an energy dispersive spectrometer (EDS).

The composition of the samples was investigated by thermogravimetric analysis (TGA) and differential scanning calorimetry (DSC), carried out on a SDT Q600 analyzer. The characterization was realized from room temperature to 1,000 °C at a heating rate of 10 °C min^{-1} under synthetic air atmosphere (White Martins).

Degradation studies

The photocatalytic degradation of the substrates was carried out in a jacketed glass cylindrical photoreactor (height: 17 cm, internal diameter: 5.5 cm, useful volume: 200 mL), equipped with magnetic stirring and continuous refrigeration by water (temperature: 25 ± 2 °C). The UV-A radiation was provided by a 125 W low pressure mercury vapor lamp (NARDS), without the original glass bulb, immersed in the solution with the protection of a Pyrex® glass jacket. Under these conditions, the measured UV-A (320-400 nm) photon flux was 9.7×10^{-5} Einstein s^{-1} (uranyl-oxalate actinometry).

The solution containing an EE2/E2 mixture (200 mL, 1 mg L^{-1}) was placed in the reactor and irradiated up to 10 min, using photocatalyst mass and working pH previously optimized by factorial design. The pH of the samples was adjusted with aqueous solutions of HCl and NaOH. Aliquots were collected at intervals of 2 min, filtered through a micro glass fiber filter (0.6 μm) to remove solid material and submitted to analytical control.

Analysis

The degradation of E2 and EE2 was monitored by high performance liquid chromatography with diode array detection (HPLC-DAD, 197 nm), using a Varian 920 LC equipment. Routine determinations were carried out on a Varian Microsorb-MV100-5 C18 column (250 × 4.6 mm, 5 μm), using a Metaguard pursuit 5 μm C-18 (4.6 mm) pre-column. The mobile phase was constituted of acetonitrile:water (50:50 v/v, isocratic mode) and used at a flow rate of 0.8 mL min^{-1}. Analytical curves were established between 0.1 and 1 mg L^{-1} ($n = 10$, $R^2 > 0.99$).[25]

Results and Discussion

The synthesized nanocomposite (TiO_2-AC) and the raw materials (sol-gel TiO_2 and AC) were firstly characterized by XRD (Figure 2). As a reference, Degussa P25 TiO_2 (Figure 2a) was also characterized, showing a sharper and stronger peak at 2θ = 25.3 corresponding to the (101) plane of the anatase structure of titania. Other less intense anatase peaks were observed at 2θ values of 36.8 (103), 37.8 (004), 38.5 (112), 48.0 (200), 54.0 (105), 55.2 (211), 62.6 (204), 68.8 (116), 70.2 (220) and 75.0 (215). Lower intensity peaks at 27.4 (110), 35.9 (101), 41.2 (111) and 56.5 (220) were assigned to the rutile phase.[26]

In general, it is accepted that pure anatase phase is more catalytically active than rutile.[27,28] Nevertheless, it is also recognized that anatase/rutile mixtures, as observed in Degussa P25-TiO_2, shows synergistic effects, which enhances the photocatalytic activity, due to the reduction of the electron/hole recombination.[29,30]

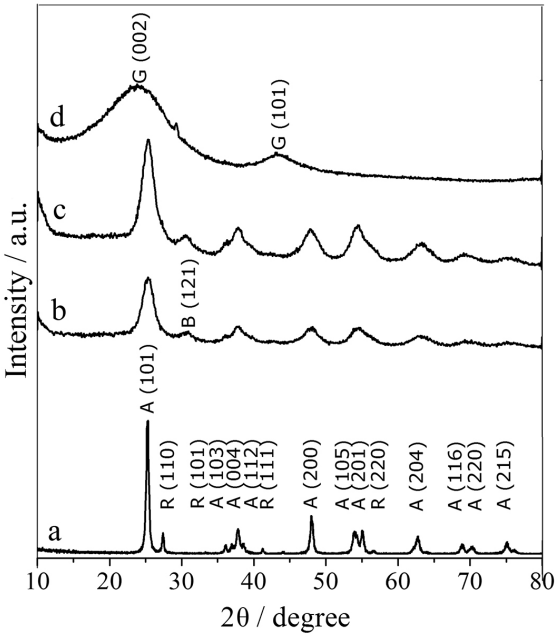

Figure 2. XRD pattern of (a) TiO_2-P25; (b) sol-gel TiO_2; (c) TiO_2-AC and (d) raw AC.

In the X-ray diffraction patterns of sol-gel TiO_2 (Figure 2b) and TiO_2-AC nanocomposite (Figure 2c) anatase appears as a dominant phase (71.9% for sol-gel TiO_2 and 80.2% for TiO_2-AC). The small signal at 2θ = 30.5 (121) was assigned to brookite (16.4% for sol-gel TiO_2 and 14.0% for TiO_2-AC) while less intense rutile peaks were observed at 2θ values of 27.4 (11.7% for sol-gel TiO_2 and 5.8% for TiO_2-AC). A preliminary interpretation about the effect caused by the presence of brookite is a very difficult task, due to the existence of reports about its low photochemical activity,[31] its "superior photoactivity"[32] and the synergistic effect of anatase/brookite mixtures.[33] Recently, Di Paola *et al.*[32] published a review about the "least known" brookite phase. According to these authors, the use of pure brookite in heterogeneous photocatalysis is not justifiable, by reason of the laborious preparation methods. In contrast, the use of mixtures of brookite with anatase and/or rutile proves to be interesting, due to a synergetic effect that hinders the electron/hole

pair combination and improves the overall efficiency of the photochemical process.

Furthermore, broad peaks suggest smaller particle size for sol-gel TiO_2 and TiO_2-AC nanocomposite, with typical anatase crystallite size of approximately 10 nm (based on the Scherrer's equation).[22] Since photocatalysis is essentially a surface phenomenon, the overall efficiency of the process tends to be significantly influenced by the particle size of the photocatalyst.[34] Consequently, it is expected that the synthesized materials shows higher photocatalytic performance than the commercial Degussa P25 TiO_2 (crystallite size around 40 nm), even with a less favorable crystalline phase ratio.

The X-ray diffraction patterns of AC (Figure 2d) shows two broad peaks at $2\theta = 23.8$ and 43.2, which can be assigned to the characteristic (002) and (101) planes.

The Raman spectra presented on Figure 3 confirms the XRD data, demonstrating the presence of anatase (A), brookite (B) and rutile (R) in the synthesized materials. The AC and TiO_2-AC spectra is characteristic of disordered carbon, showing two bands centered at approximately 1,600 (G) and 1,340 cm^{-1} (D).

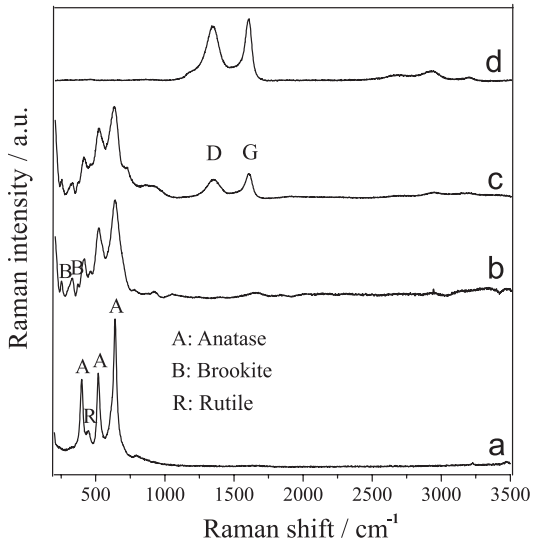

Figure 3. Raman spectra of (a) TiO_2-P25; (b) sol-gel TiO_2; (c) TiO_2-AC and (d) raw AC.

The I_D/I_G ratio is often used to evaluate the disorder of carbon materials,[35] where I_D represents the intensity of the D band (which is associated with the disorder) due to the breathing carbon bonded modes that require a defect for its activation, and I_G represents the intensity of the high frequency E_{2g} phonon at the Brillouin zone center (G band), which is characteristic of sp^2 carbon.[36,37] The raw AC shows an estimated I_D/I_G of 2.1, which corresponds to substantially disordered carbon. Besides, the presence of TiO_2 in the nanocomposite increased the estimated value of this ratio (2.9), which suggests the introduction of significant changes in the structure of the starting material and, consequently, an intimate contact between the photocatalyst and the carbonaceous matrix.

The superficial morphology of AC, TiO_2-P25, sol-gel TiO_2 and TiO_2-AC powders was evaluated by scanning electron microscopy (SEM), and the results are shown in Figure 4. In the SEM images of activated carbon (AC) it is observed a typical porous and rough surface, while TiO_2-P25 images show aggregates of spherical-shaped particles, similar to the observed by Jo and Kang.[38] The images of the sol-gel TiO_2 also show particle agglomeration, however, with irregular distribution and smaller dimensions than the commercial product. Finally, the SEM image of the TiO_2-AC nanocomposite shows agglomerates of titanium dioxide nanoparticles covering the whole surface of the carbonaceous matrix.

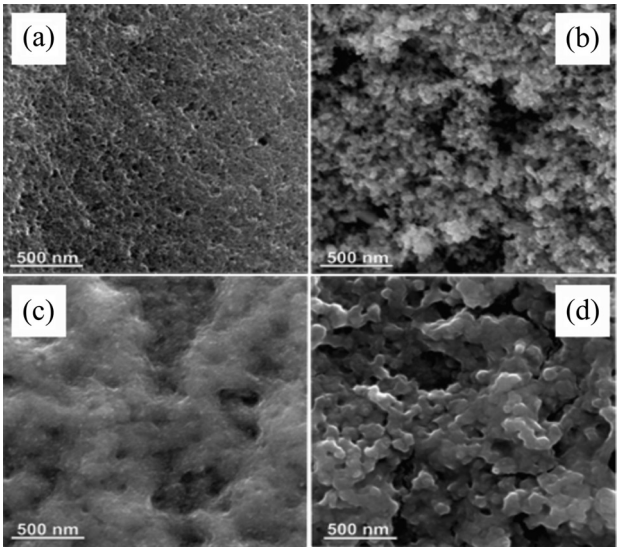

Figure 4. SEM images of (a) AC; (b) TiO_2-P25; (c) sol-gel TiO_2; (d) TiO_2-AC (magnification 100,000×).

The carbon mass in the synthesized nanocomposite was estimated by thermogravimetric analysis (TGA). As shown in Figure 5, when the TiO_2-AC is heated from the room temperature to 1,000 °C in an air flow, the TG curve shows three-step of weight loss. The first thermal event appears between 23-154 °C with a weight loss of 9.1 wt.%, probably due to the endothermic removal of physically and chemically adsorbed water from the TiO_2 nanoparticles.[39,40] In the second step, a weight loss of 6.5 wt.% at the temperature range of 154-419 °C may be associated with the decomposition of amorphous carbon layers and loss of hydroxyl groups on the TiO_2 nanocrystal,[40,41] and the final weight loss from 419 to 616 °C (3.9 wt.%) refers to an exothermic process and can be attributed to the combustion of carbon[39] and to the anatase to rutile phase transition.[42]

In the thermal characterization of AC, an exothermic event was observed between 352 and 583 °C, with a high weight loss, approximately 80% (Figure S2), assigned to the combustion of carbonaceous material. The TGA/DTG (derivative thermogravimetry) of nano TiO_2 is shown in Figure S3.

Based on the previously exposed results, the carbon content on the synthesized nanocomposite was estimated in 11.4 wt.%.

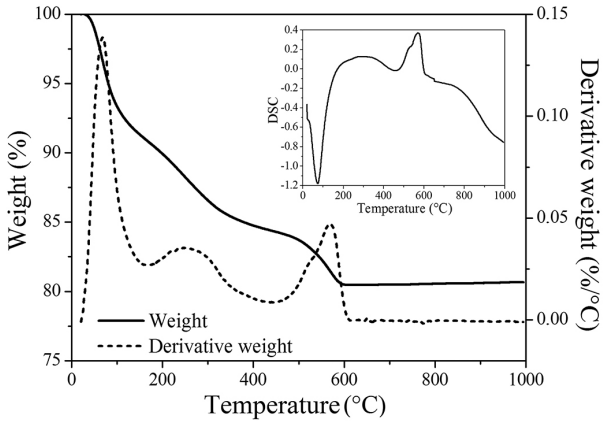

Figure 5. TGA, DTG and DSC profiles of the TiO_2-AC nanocomposite.

Photocatalytic activity

Initially, the effects of two relevant operational variables (pH and catalyst concentration) were evaluated by a factorial design (2^2), using TiO_2 Degussa P25 as a model photocatalyst, a mixture of E2 and EE2 (1 mg L^{-1}) as substrate and photocatalytic processes assisted by artificial UV-A radiation (i.e., mercury vapor lamp). In this study (Table S1, Supplementary Information), higher degradation efficiency was observed at pH 6 using 250 mg L^{-1} of photocatalyst, condition employed in all subsequent studies.

Under these conditions, the UV-A photolytic degradation of both estrogens was similar, reaching values of about 30% in exposure times of 10 min (Figure 6). Although many studies show a significant degradation of estrogens by direct photolysis,[43] it is admitted that their contribution in photocatalytic processes is less relevant. Furthermore, many studies report the photolytic formation of reaction intermediates that can exhibit greater toxicity than the starting compounds.[44]

The adsorption capacity shown by TiO_2-P25 and the synthesized TiO_2 nanoparticles was quite similar, allowing removals lower than 5% for both estrogens. This result is consistent with the low porosity of these materials, as highlighted by García-Muñoz *et al.*[45] As expected, the adsorption capacity shown by the TiO_2-AC nanocomposite was larger (removal near 30% in contact time of 10 min), due to the characteristic high porosity and surface area of the carbonaceous materials.

In photocatalytic processes the degradation efficiency of TiO_2-P25 was superior, allowing almost complete removal of both estrogens in treatments of 4 min. The linear correlation between ln (C/C_0) and t ($\ln C/C_0 = k_{appt}\, t$, where C_0 represents the initial concentration and C represents the concentration at a particular time, t) indicates that the photocatalytic degradation follows a pseudo first-order kinetics, with apparent rate constants (k_{app}) of approximately 1 min^{-1}. In the presence of TiO_2 nanoparticles the degradation process was slower (k_{app} ca. 0.5 min^{-1}), requiring treatment times of 8 min to complete estrogen's removal.

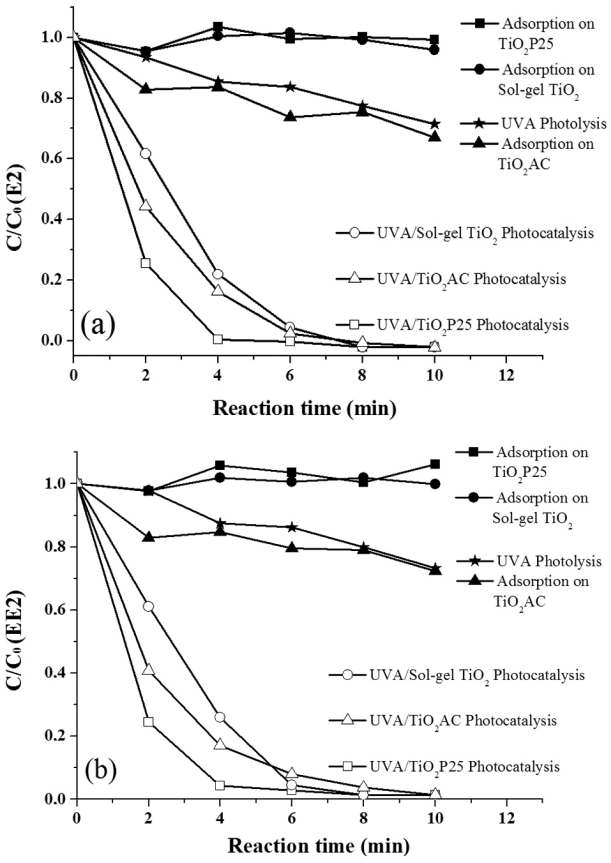

Figure 6. Removal of E2 (a) and EE2 (b) by the indicated processes (estrogens: 1 mg L^{-1}, volume: 0.2 L, pH: 6, catalyst: 250 mg L^{-1}).

The superiority of the commercial TiO_2-P25, even with smaller surface area, demonstrates that the photocatalytic activity is not only dependent on the particle size, being governed by other important characteristics, such as availability of active sites.[46] A complementary explanation for the higher photocatalytic activity of TiO_2-P25 is based on the composition of crystalline phases. The commercial product consists in a mixture of anatase (80%) and rutile

(20%), with a recognized synergistic effect,[47,48] while the synthesized TiO_2 nanoparticles comprise a mixture of anatase (71.9%), brookite (16.4%) and rutile (11.7%), with lower photochemical activity.

The AC presence in the nanocomposite containing TiO_2 nanoparticles causes a slight increase in the degradation capacity of the photocatalytic process (k_{app} ca. 0.6 min^{-1}). However, due to the higher adsorption capacity introduced by AC, this effect cannot be considered as synergistic.

This result disagrees with many reports that describe an important synergistic effect between these components.[8,14,45,49,50] Although there is a consensus on this synergistic effect, assuming that the presence of AC favors the approximation between substrate and photocatalyst, there are additional arguments that suggest a much more complex effect. According to Cordero *et al.*[51] the differences in the photoactivity of TiO_2 depends on the physicochemical properties of activated carbons, particularly the existence of active sites on their surface. In studies involving the degradation of 4-chlorophenol it was observed that L-type AC can induce beneficial or unfavorable effects on the TiO_2 activity, depending on the presence of organic functional groups (i.e., carboxylic acid groups) that can transfer electronic density to the TiO_2, thus inhibiting the recombination process.

According to observations carried out by Asenjo *et al.*[52] the apparent synergy between the activated carbon and TiO_2 particles, claimed by several authors, is resulting from an incorrect use of the first-order form of the Langmuir-Hinshelwood (LH) equation. In studies involving the photocatalytic degradation of phenol, the authors showed that the use of the extended form of the LH equation demonstrates that the synergy is only apparent.

Finally, it is important to remark that many studies do not show adequate experimental controls in order to verify, for instance, the contribution of concomitant processes such as photolysis and adsorption. Furthermore, some studies compare the photocatalytic efficiency of TiO_2/AC and pure TiO_2 using the same mass of TiO_2, while others may use the same overall mass.[14]

Conclusions

Sol-gel TiO_2 and TiO_2-AC nanocomposite were prepared by sol-gel methods. Both materials showed high degradation efficiency of E2 and EE2 estrogens, allowing removal greater than 90% at reaction times of 6 min. Commercial TiO_2-P25 showed higher degradation efficiency than the synthesized sol-gel TiO_2, probably because of its more favorable anatase/rutile ratio. Under the conditions of this study, no synergistic effect was observed.

Supplementary Information

Supplementary data are available free of charge at http://jbcs.sbq.org.br as PDF file.

Acknowledgments

Financial support from CNPq, CAPES, NENNAM (Pronex F. Araucária/CNPq) and Fundação Araucária is gratefully acknowledged.

References

1. Babuponnusami, A.; Muthukumar, K.; *J. Environ. Chem. Eng.* **2014**, *2*, 557.
2. Fujishima, A.; Zhang, X.; Tryk, D. A.; *Int. J. Hydrogen Energy* **2007**, *32*, 2664.
3. Loaiza-Ambuludi, S.; Panizza, M.; Oturan, N.; Oturan, M. A.; *Catal. Today* **2014**, *224*, 29.
4. Nakata, K.; Fujishima, A.; *J. Photochem. Photobiol., C* **2012**, *13*, 169.
5. Bianchi, C. L.; Colombo, E.; Gatto, S.; Stucchi, M.; Cerrato, G.; Morandi, S.; Capucci, V.; *J. Photochem. Photobiol., A* **2014**, *280*, 27.
6. De la Cruz, N.; Dantas, R. F.; Giménez, J.; Esplugas, S.; *Appl. Catal., B* **2013**, *130-131*, 249.
7. Coleman, H. M.; Abdullah, M. I.; Eggins, B. R.; Palmer, F. L.; *Appl. Catal., B* **2005**, *55*, 23.
8. Shan, A. Y.; Ghazi, T. I. M.; Rashid, S. A.; *Appl. Catal., A* **2010**, *389*, 1.
9. Shen, C.; Wang, Y. J.; Xu, J. H.; Luo, G. S.; *Chem. Eng. J.* **2012**, *209*, 478.
10. Nakano, R.; Chand, R.; Obuchi, E.; Katoh, K.; Nakano, K.; *Chem. Eng. J.* **2011**, *260*, 176.
11. Amereh, E.; Afshar, S.; *Mater. Chem. Phys.* **2010**, *120*, 356.
12. Hu, C.; Duo, S.; Liu, T.; Xiang, J.; Li, M.; *Appl. Surf. Sci.* **2011**, *257*, 3697.
13. Panniello, A.; Curri, M. L.; Diso, D.; Licciulli, A.; Locaputo, V.; Agostiano, A.; Comparelli, R.; Mascolo, G.; *Appl. Catal., B* **2012**, *190*, 122.
14. Leary, R.; Westwood, A.; *Carbon* **2011**, *49*, 741.
15. Gao, B.; Yap, P. S.; Lim, T. M.; Lim, T. T.; *Chem. Eng. J.* **2011**, *171*, 1098.
16. Ravichandran, L.; Selvam, K.; Swaminathan, M.; *J. Mol. Catal. A: Chem.* **2010**, *317*, 89.
17. Gu, L.; Chen, Z.; Sun, C.; Wei, B.; Yu, X.; *Desalination* **2010**, *263*, 107.
18. Silva, C. G.; Wang, W.; Faria, J. L.; *J. Photochem. Photobiol., A* **2006**, *181*, 314.
19. Luo, Y.; Guo, W.; Ngo, H. H.; Nghiem, L. D.; Hai, F. I.; Zhang, J.; Liang, S.; Wang, X. C.; *Sci. Total Environ.* **2014**, *473-474*, 619.

20. Silva, C. P.; Otero, M.; Esteves, V.; *Environ. Pollut.* **2012**, *38*, 165.
21. Oliveira, M. M.; Schnitzler, D. C.; Zarbin, A. J. G.; *Chem. Mater.* **2003**, *15*, 1903.
22. Mandal, S. S.; Bhattacharyya, A. J.; *Talanta* **2010**, *82*, 876.
23. Zhang, H.; Banfield, J. F.; *J. Phys. Chem. B* **2000**, *104*, 3481.
24. Wang, Z.; Lu, Z.; Huang, Y.; Xue, R.; Huang, X.; Chen, L.; *J. Appl. Phys.* **1997**, *82*, 5705.
25. Marinho, B. A.; de Liz, M. V.; Lopes Tiburtius, E. R.; Nagata, N.; Peralta-Zamora, P.; *Photochem. Photobiol. Sci.* **2013**, *12*, 678.
26. Venkatachalam, S.; Hayashi, H.; Ebina, T.; Nanjo, H.; *Optoelectronics - Advanced Materials and Devices*; Pyshkin, S., ed.; InTech: Rijeka, 2013, ch. 5.
27. Aruldoss, U.; Kennedy, L. J.; Judith Vijaya, J.; Sekaran, G.; *J. Colloid Interface Sci.* **2011**, *355*, 204.
28. Hofer, M.; Penner, D.; *J. Eur. Ceram. Soc.* **2011**, *31*, 2887.
29. van der Meulen, T.; Mattson, A.; Österlund, L.; *J. Catal.* **2007**, *251*, 131.
30. Liao, J.; Luo, R.; Li, Y. B.; Zhang, J.; *Mater. Sci. Semicond. Process.* **2013**, *16*, 2032.
31. Zhang, J.; Yan, S.; Fu, L.; Wang, F.; Yuan, M.; Luo, G.; Xu, Q.; Wang, X.; Li, C.; *Chin. J. Catal*. **2011**, *32*, 983.
32. Di Paola, A.; Bellardita, M.; Palmisano, L.; *Catalyst* **2013**, *3*, 36.
33. Yu, J. C.; Zhang, L.; Yu, J.; *Chem. Mater.* **2002**, *14*, 4647.
34. Alzamani, M.; Shokuhfar, A.; Eghdam, E.; Mastali, S.; *Prog. Nat. Sci.* **2013**, *23*, 77.
35. Tai, F. C.; Lee, S. C.; Wei, C. H.; Tyan, S. L.; *Mater. Trans.* **2006**, *47*, 1847.
36. Cançado, L. G.; Jorio, A.; Ferreira, E. H. M.; Stavale, F.; Achete, C. A.; Capaz, R. B.; Moutinho, M. V. O.; Lombardo, A.; Kulmala, T. S.; Ferrari, A. C.; *Nano Lett.* **2011**, *11*, 3190.
37. Ferrari, A. C.; Basko, D. M.; *Nat. Nanotechnol.* **2013**, *8*, 235.
38. Jo, W.-K.; Kang, H.-J.; *Mater. Chem. Phys.* **2013**, *143*, 247.
39. Gundogdu, A.; Duran, C.; Senturk, H. B.; Soylak, M.; Imamoglu, M.; Onal, Y.; *J. Anal. Appl. Pyrolysis* **2013**, *104*, 249.
40. Xia, T.; Zhang, W.; Wang, Z.; Zhang, Y.; Song, X.; Murowchick, J.; Battaglia, V.; Liu, G.; Chen, X.; *Nano Energy* **2014**, *6*, 109.
41. Hu, Y.; Tsai, H. L.; Huang, C. L.; *J. Eur. Ceram. Soc.* **2003**, *23*, 691.
42. Liu, X.; *Powder Technol.* **2012**, *224*, 287.
43. Li Puma, G.; Puddu, V.; Tsang, H. K.; Gora, A.; Toepfer, B.; *Appl. Catal., B* **2010**, *99*, 388.
44. Chowdhury, R. R.; Charpentier, P. A.; Ray, M. B.; *J. Photochem. Photobiol., A* **2011**, *219*, 67.
45. García-Munõz, P.; Carbajo, J.; Faraldos, M.; Bahamonde, A.; *J. Photochem. Photobiol., A* **2014**, *287*, 8.
46. Carp, O.; Huisman, C. L.; Reller, A.; *Prog. Solid State Chem.* **2004**, *32*, 33.
47. Tian, G.; Fu, H.; Jing, L.; Tian, C.; *J. Hazard. Mater.* **2009**, *161*, 1122.
48. Li, G.; Gray, K. A.; *Chem. Phys.* **2007**, *339*, 173.
49. Rivera-Utrilla, J.; Sánchez-Polo, M.; Abdel daiem, M. M.; Ocampo-Pérez, R.; *Appl. Catal., B* **2012**, *126*, 100.
50. Kavitha, R.; Devi, L. G.; *J. Environ. Chem. Eng.* **2014**, *2*, 857.
51. Cordero, T.; Duchamp, C.; Chovelon, J. M.; Ferronato, C.; Matos, J.; *J. Photochem. Photobiol., A* **2007**, *191*, 122.
52. Asenjo, N. G.; Santamaría, R.; Blanco, C.; Granda, M.; Álvarez, P.; Menéndez, R.; *Carbon* **2013**, *55*, 62.

Submitted: March 16, 2016
Published online: July 5, 2016